ACS APPLIED NANO MATERIALS

www.acsanm.org Forum Article

# Zeolitic Imidazolate Framework Nanoencapsulation of CpG for Stabilization and Enhancement of Immunoadjuvancy

Olivia R. Brohlin, Ryanne N. Ehrman, Fabian C. Herbert, Yalini H. Wijesundara, Arun Raja, Arezoo Shahrivarkevishahi, Shashini D. Diwakara, Ronald A. Smaldone, and Jeremiah J. Gassensmith*

Cite This: https://doi.org/10.1021/acsanm.1c03555

Read Online

ACCESS | Metrics & More | Article Recommendations

**ABSTRACT:** Metal−organic frameworks (MOFs) have been used to improve vaccine formulations by stabilizing proteins and protecting them against thermal degradation. This has led to increased immunogenicity of these proteinaceous therapeutics. In this work, we show that MOFs can also be used to protect the single-stranded DNA oligomer CpG to increase its immunoadjuvancy. By encapsulation of the phosphodiester CpG in the zinc-based MOF, zeolitic imidazolate framework-8, the DNA oligomer is protected from nuclease degradation and exhibits improved cellular uptake. As a result, we have been able to achieve drastically enhanced B-cell activation in splenocyte cultures comparable to the current state-of-the-art phosphorothioate CpG. Furthermore, we have made a direct comparison of micro- and nanosized MOFs for optimization of the particulate delivery of immunoadjuvants to maximize immune activation.

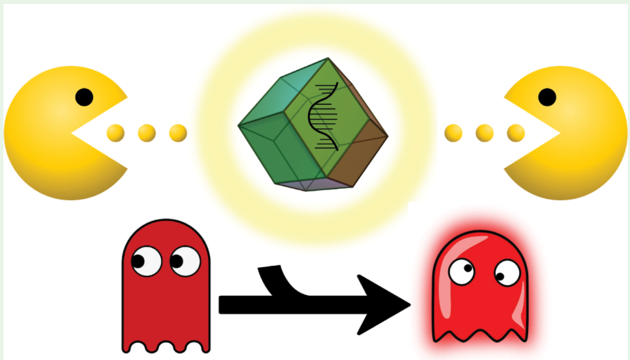

**KEYWORDS:** *metal−organic framework, zeolitic imidazolate framework 8, CpG, immunoadjuvant, phosphodiester DNA, B cell activation, nuclease resistance*

Downloaded via UNIV OF TEXAS AT DALLAS on January 31, 2022 at 21:52:30 (UTC).
See https://pubs.acs.org/sharingguidelines for options on how to legitimately share published articles.

## ■ INTRODUCTION

Metal−organic frameworks (MOFs) have been used to stabilize a wide variety of biomacromolecules including proteins,[1,2] viruses,[3] and liposomes[4] against thermal degradation as a means to overcome the "cold chain". This technology has been revolutionary in overcoming the notorious instability of biological therapeutics and offers the possibility of significantly reducing their cost and increasing their accessibility, specifically in developing areas that lack the infrastructure to maintain the required refrigeration for storage and transport.[5,6] These powerful polymeric frameworks are formed through coordination bonds between a metal node and organic linkers.[7−9] Biomacromolecules act as nucleating agents that catalyze MOF formation, resulting in encapsulation through a process called biomimetic mineralization.[10−13] Once encapsulated, the biomacromolecule is protected from enzymatic degradation[14] and thermal denaturation.[15,16] The resulting structure is thermodynamically stable[17−19] but is kinetically labile and easily degrades in the presence of strong metal chelators,[20,21] low pH,[22,23] and inorganic phosphates,[24] which allows for the recovery of the preserved biomacromolecule. In this work, we apply this technology for encapsulation of the single-stranded DNA (ssDNA) immunoadjuvant CpG.

Vaccines often have a limited ability to activate the B- and T-cell-mediated components of the immune system and therefore must be combined with an immunoadjuvant to promote and direct the immune response.[25−27] Synthetic adjuvants designed to mimic pathogen-associated molecular patterns (PAMPs) can bind to pattern recognition receptors to begin the process of switching immune cells from a passive naive state to an active state ready to fight infection.[28,29] CpG is a synthetic immunoadjuvant composed of unmethylated, bacterial ssDNA.[30,31] In mammals, 70−80% of CpG cytosines are methylated; therefore, unmethylated CpG is recognized by the immune system as a PAMP.[32,33] The immunoadjuvant CpG can activate both plasmacytoid dendritic cells (pDCs) and B cells to trigger a proinflammatory response.[34] This is important because pDCs are the body's vanguards against infection by foreign pathogens and proliferation of cancer, while B cells are responsible for producing different types of proteins that bind

**Special Issue:** Professor Sir Fraser Stoddart's 80th Birthday Forum

**Received:** October 22, 2021
**Accepted:** December 30, 2021

ACS Publications © XXXX American Chemical Society

**Scheme 1. Illustration of the Encapsulation of CpG in ZIF-8 for Enhanced Immunoadjuvancy[a]**

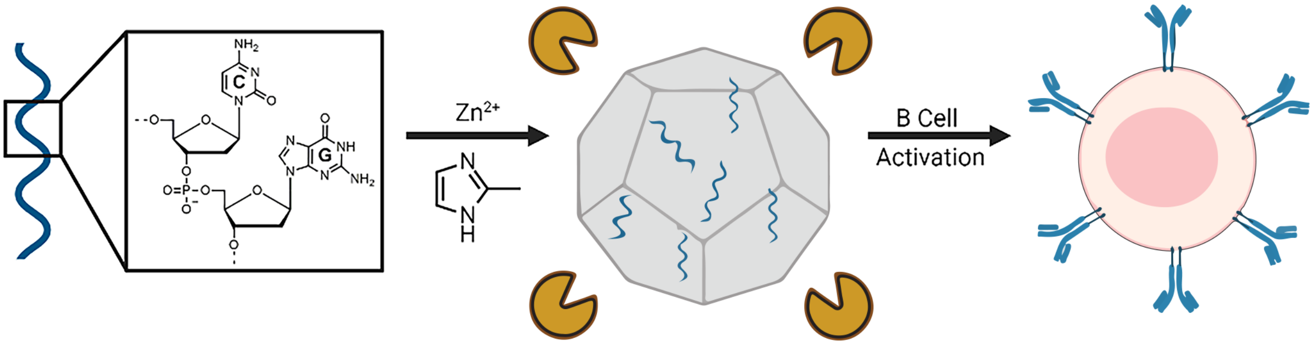


[a]The ssDNA immunoadjuvant CpG is encapsulated in the zinc-based MOF ZIF-8 by biomimetic mineralization using $Zn^{2+}$ and HMIM. Encapsulation of CpG within ZIF-8 affords nucleic acid protection from nucleases and promotes cellular uptake for enhanced B cell activation.

to and neutralize infection, in particular, different types of immunoglobulins or antibodies.

There are two main types of CpG, each specializing in activating a specific part of the innate immune system. Class A CpG (also referred to as D-type) more strongly activates pDCs and promotes a T-cell-mediated cellular immune response,[35] whereas class B CpG (K-type) more strongly activates B cells and promotes a humoral immune response.[36] Because of their ability to boost antibody production, class B CpG immunoadjuvants have been the focus of human clinical trials for vaccines, infectious diseases, and cancer.[37−39] The major limitation undermining the success of CpG in clinical trials comes from the nuclease susceptibility of the DNA backbone.[40] The current state-of-the-art technology has reengineered the labile phosphodiester (PO) backbone by thiolation of the sugar moiety to form a nuclease-resistant phosphorothioate (PS) bond, resulting in an increased *in vivo* half-life of 30−60 min (5−10 min for PO).[41] However, this modification has been found to lower the immunoadjuvancy of CpG and induce acute toxicity.[42,43]

As an alternative to PS backbone modification, we propose using MOFs to improve the *in vivo* stability of PO CpG. In this way, we can protect CpG from nucleases while also retaining the innate immunoadjuvancy of the oligonucleotide. Recent work with zeolitic imidazolate framework 8 (ZIF-8), a zinc-based MOF, has shown it to be possible to grow a MOF shell around biomacromolecules in a simple one-pot synthesis under ambient conditions.[44−47] The resulting formulation does not require refrigeration, unlike other currently used nanocarriers such as lipid nanoparticles,[48] virus-like particles,[49] and liposomes.[50] ZIF-8 forms a protective barrier that inhibits the enzymatic degradation of biomacromolecules.[51] ZIF-8 has previously served[52] as a nanoparticle carrier of PS CpG by electrostatically binding the negatively charged CpG onto the cationic surface of the crystals to promote cellular uptake and enhance immunoadjuvancy in macrophages. In this work, we encapsulate PO CpG within ZIF-8 to protect the DNA from nucleases and enhance immunoadjuvancy by improving B cell activation (Scheme 1). Furthermore, we have optimized our formulation by tuning the ZIF-8 metal-to-ligand ratios to synthesize both micro- and nanosized CpG@ZIF.

## ■ EXPERIMENTAL SECTION

**Materials.** PO CpG (ODN 1826-Class B) and fluorescein isothiocyanate (FITC)-labeled PO CpG were purchased as custom DNA oligomers from Invitrogen [Waltham, MA; sequence 5′-tccatgacgttcctgacgtt-3′ (20 mer); 5′ FAM modification]. PS CpG (ODN 1826), FITC-labeled PS CpG (ODN 1826 FITC), and PS GpC (ODN 1826 control: ODN 2138) were purchased from InvivoGen (San Diego, CA). Nuclease-free water, zinc acetate dihydrate, 2-methylimidazole, β-mercaptoethanol, RPMI-1640, Dulbecco's modified Eagle's medium (DMEM), FB Essence, penicillin−streptomycin, phosphate-buffered saline, and desoxyribonuclease I (DNase I) were purchased from Sigma-Aldrich (St. Louis, MO), Thermo Fisher Scientific (Waltham, MA), or VWR (Radnor, PA). Lactate dehydrogenase (LDH) cytoxicity assay kit, cell staining buffer, RBC lysis buffer, Alexa Fluor 700 antimouse CD19 antibody, Alexa Fluor 647 antimouse CD80 antibody, and PE antimouse CD86 antibody were purchased from BioLegend (San Diego, CA).

**CpG@ZIF Synthesis and Characterization.** *Synthesis of CpG@ZIF.* Stock solutions of 1 M $Zn(OAc)_2$ and 3 M 2-methylimidazole (HMIM) were made in nuclease-free water. For the synthesis of CpG@μZIF, 213 μL of 3 M HMIM (final concentration 640 mM) was combined with 708 μL of nuclease-free water. A total of 39 μL of 100 μM PO CpG (final concentration 25 μg/mL) was added, and the solution was vortexed for 10 s. Last, 40 μL of 1 M $Zn(OAc)_2$ (final concentration 40 mM) was added, and the solution was vortexed for another 30 s. The solution immediately turned turbid and was allowed to react at room temperature (RT) for 1 h. The same was done for the synthesis of CpG@nZIF using 853 μL of 3 M HMIM (final concentration 2560 mM), 28 μL of nuclease-free water, 39 μL of 100 μM PO CpG (final concentration 25 μg/mL), and 80 μL of 1 M $Zn(OAc)_2$ (final concentration 80 mM). For the synthesis of pristine ZIF, the same conditions were used except 39 μL of additional nuclease-free water was added in place of 39 μL of PO CpG. The resulting solutions were centrifuged at 17000*g* for 10 min to obtain a pellet of the crystals. The crystals were then washed with 1000 μL of methanol (MeOH), a mixture of 500 μL of MeOH and 500 μL of nuclease-free water, and 1000 μL nuclease-free water using the same centrifugation method. The final pellet was resuspended in nuclease-free water. The same procedure was used for the encapsulation of FITC-labeled CpG. For adsorption of CpG onto the surface of ZIF (CpG+ZIFs), 39 μL of 100 μM PO CpG was combined with pristine ZIF in a total reaction volume of 100 μL and incubated on a rotisserie for 1 h at RT. The samples were purified by centrifugation (17000*g* for 10 min); however, no subsequent washings were employed to prevent dislodging of the surface-adsorbed CpG.

*Characterization of CpG@ZIF. Scanning Electron Microscopy (SEM).* The surface morphology of the CpG@ZIFs was examined using a Zeiss Supra 40 scanning electron microscope at 2.5 kV and 6−10 mm working distance. A total of 5 μL of the prepared crystals in nuclease free water was loaded onto a silicon wafer and allowed to dry for 10 s, and the excess was wicked off using Whatman Filter Paper No. 1. The samples were then sputtered with a ∼40 Å layer of gold before being imaged.

*Dynamic Light Scattering (DLS).* The size and polydispersity of the CpG@ZIFs were quantified using a Malvern Analytical Zetasizer Nano ZS. A total of 1 mL of the crystals diluted in nuclease-free water


https://doi.org/10.1021/acsanm.1c03555
ACS Appl. Nano Mater. XXXX, XXX, XXX−XXX

was loaded into a 1 mL disposable cuvette and read at 25 °C, a 175° scattering angle, a medium refractive index of 1.33, a 633 nm laser, and a material refractive index of 1.51.

*ζ Potential.* The charge of the CpG@ZIFs was quantified using a Malvern Analytical Zetasizer Nano ZS. A total of 1 mL of the crystals diluted in nuclease-free water was loaded into a 1 mL disposable folded capillary cell and read at 25 °C.

*Powder X-ray Diffraction (PXRD).* The crystallinity of the CpG@ZIFs was determined with a Rigaku SmartLab X-ray diffractometer with Cu Kα (1.54060 Å) at 30 mA and 40 kV. The samples were washed with MeOH and put under vacuum overnight before being analyzed.

*Brunauer−Emmett−Teller (BET) Nitrogen Isotherms.* The surface areas of the CpG@ZIFs were quantified using a Micrometrics ASAP 2020 surface area analyzer. Nitrogen adsorption measurements were taken at 77 K. The samples were activated in MeOH for 4 h, dried under vacuum for 24 h, soaked with dichloromethane for 4 h, and finally dried under vacuum for another 24 h. Before analysis, the samples were put under vacuum and degassed at 120 °C for 12 h. The data were processed by the BET method for calculation of the surface area, and the pore sizes were quantified by nonlocalized density functional theory with a carbon slit pore model.

*Confocal Microscopy.* The fluorescence of the FITC-labeled PO CpG encapsulated in ZIF-8 was qualitatively observed using an Olympus FV3000 RS confocal microscope. A total of 10 μL of the sample was loaded onto a glass slide, covered with a glass coverslip, and left to dry overnight in the dark. The slide was then sealed and imaged using 100× magnification. Images were processed using *ImageJ* software.

*Fluorimetry.* The encapsulation efficiency of FITC-labeled PO CpG in ZIF-8 before and after denaturing washes was quantified by measuring the FITC fluorescence intensity of the supernatant during synthesis. For washing, CpG@ZIFs were treated with either 10% Sodium dodecyl sulfate (SDS) for 30 min at RT or 2 units of DNase I for 10 min at 37 °C. After, the solution was centrifuged at 17000*g* for 10 min, and 100 μL of the supernatant was added to a black 96-well plate in triplicate. Fluorescence readings at $\lambda_{ex}$ = 495 nm and $\lambda_{em}$ = 520 nm were performed on a BioTek Synergy H4 hybrid microplate reader. The encapsulation efficiency was calculated as a percent of the FITC fluorescence intensity of the starting material.

**CpG@ZIF Stability against DNase I.** The digestion was performed according to the manufacturer's protocol. In brief, 10 μg each of encapsulated and unencapsulated PO CpG (as well as PS CpG) were incubated with 1 μL (2 units) of DNase I and 10 μL of 10× DNase reaction buffer (final concentration 1×) in a final reaction volume of 100 μL using nuclease-free water. The mixture was incubated for 10 min at 37 °C. The reaction was quenched with 1 μL of 0.5 M ethylenediaminetetraacetic acid (EDTA). The digested and undigested CpG@ZIFs samples were centrifuged at 17000*g* for 10 min and the supernatants decanted. A total of 100 μL of 0.5 M EDTA was used to dissolve the ZIF-8 crystals and recover CpG. The recovered CpG samples were run on a 5% agarose gel containing 0.5 mg/mL ethidium bromide at 100 V for 10 min with a 1× TBE running buffer alongside an ultralow-range DNA ladder. The same was done for the adsorbed samples (CpG+ZIFs) except EDTA exfoliation was not required to recover CpG.

**CpG@ZIF Performance *in Vitro*.** *Cytotoxicity.* Cell viability assay was performed according to the manufacturer's protocol. In brief, RAW 264.7 murine macrophages were grown in DMEM supplemented with 10% FB Essence and 1% penicillin−streptomycin. The cells were then seeded at a concentration of $1 \times 10^6$ cells/mL in a 96-well plate (100 μL/well) and allowed to adhere overnight. All incubations took place in a 37 °C $CO_2$ incubator. The following day the cells were treated with the CpGs, CpG@ZIFs, or ZIFs at a CpG concentration of 3.3 μg/mL (100 μL/well) for 4 h. Next, 10 μL of lysis buffer was added to a set of untreated cells for 30 min to create the negative control. After that, 100 μL of the working solution was added to all of the wells for 30 min in a light-protected area. Last, 50 μL of the stop solution was added to all wells before the absorbance was read at 490 nm on a BioTek Synergy H4 hybrid microplate reader.

*Uptake.* Spleens from naïve BALB/c mice were collected from euthanized mice in accordance with Protocol 19-06 approved by the Institutional Animal Care and Use Committee (IACUC), The University of Texas at Dallas. Spleens were homogenized into single-cell suspensions using cell pestles and 100 μm cell strainers, and red blood cells were lysed with 1× RBC lysis buffer. Splenocytes were seeded at $1 \times 10^6$ cells/mL in a 24-well plate (2 mL/well). The splenocytes were treated with FITC-labeled CpGs, CpG@ZIFs, or ZIFs (3.3 μg/mL CpG concentration) in RPMI supplemented with 10% FB Essence, 1% penicillin−streptomycin, and 50 μM β-mercaptoethanol for 4 h at 37 °C in a $CO_2$ incubator. After that, the cells were washed three times with 0.5 M sodium acetate buffer at pH 5 to remove surface-bound material, washed three times with 1× phosphate-buffered saline (PBS), stained with Alexa Fluor 700 antimouse CD19 antibody to identify the B cells, washed three times with a cell-staining buffer, and finally resuspended in 1 mL of a cell-staining buffer. Quantitative analyses were completed using a BD LSR Fortessa flow cytometer, with approximately 100000 events collected per sample. Data processing was performed on *FlowJo* software, version 10.6.1.

*B Cell Activation.* Spleens from naïve BALB/c mice were collected from euthanized mice in accordance with Protocol 19-06 approved by the IACUC, The University of Texas at Dallas. Spleens were homogenized into single-cell suspensions using cell pestles and 100 μm cell strainers, and red blood cells were lysed with 1× RBC lysis buffer. Splenocytes were seeded at $1 \times 10^6$ cells/mL in a 24-well plate (2 mL/well). The splenocytes were treated with FITC-labeled CpGs, CpG@ZIFs, or ZIFs (3.3 μg/mL CpG concentration) in RPMI supplemented with 10% FB Essence, 1% penicillin−streptomycin, and 50 μM β-mercaptoethanol for 4 h at 37 °C in a $CO_2$ incubator. The cells were washed three times with 0.5 M sodium acetate buffer at pH 5 to remove surface-bound material, washed three times with 1× PBS, stained with Alexa Fluor 700 antimouse CD19 antibody, Alexa Fluor 647 antimouse CD80 antibody, and PE antimouse CD86 antibody to identify activated B cells, washed three times with a cell-staining buffer, and finally resuspended in 1 mL of a cell-staining buffer. Quantitative analyses were completed using a BD LSR Fortessa flow cytometer, with approximately 100000 events collected per sample. Data processing was performed on *FlowJo* software, version 10.6.1.

## ■ RESULTS AND DISCUSSION

Biomimetic mineralization of ZIF-8 on the surface of CpG was done by iteratively adjusting aqueous solutions of zinc acetate and HMIM as the metal node and organic ligand, respectively. Tuning the metal-to-ligand ratio allows us to not only capture the oligonucleotide but also control the size of ZIF-8. From our initial screen, we found that we could produce CpG encapsulated in microsized crystals (CpG@μZIF) when we used 40 mM $Zn(OAc)_2$, 640 mM HMIM, and 25 μg/mL CpG. Further, we found that when we used 80 mM $Zn(OAc)_2$, 2560 mM HMIM, and 25 μg/mL CpG, we could synthesize nanosized crystals (CpG@nZIF). Prior work using[4] time-resolved X-ray spectroscopy showed that ZIF-8 formation begins within seconds; consequently, the time that the DNA resides at these high concentrations of metals and ligand is extremely short before it becomes encapsulated. SEM micrographs of the resulting microcrystals (Figure 1A) and nanocrystals (Figure 1B) show the characteristic rhombic dodecahedral shape of ZIF-8 that is consistent with pristine ZIFs (Figure 1C,D). Furthermore, the crystallinity of the CpG@ZIFs was measured by PXRD, with the patterns matching that of pristine and simulated ZIF-8 (Figure 1E). Following activation, we found that the resulting composites were still porous. As expected, the nitrogen isotherms of CpG@μZIF and CpG@nZIF show diminished surface areas,

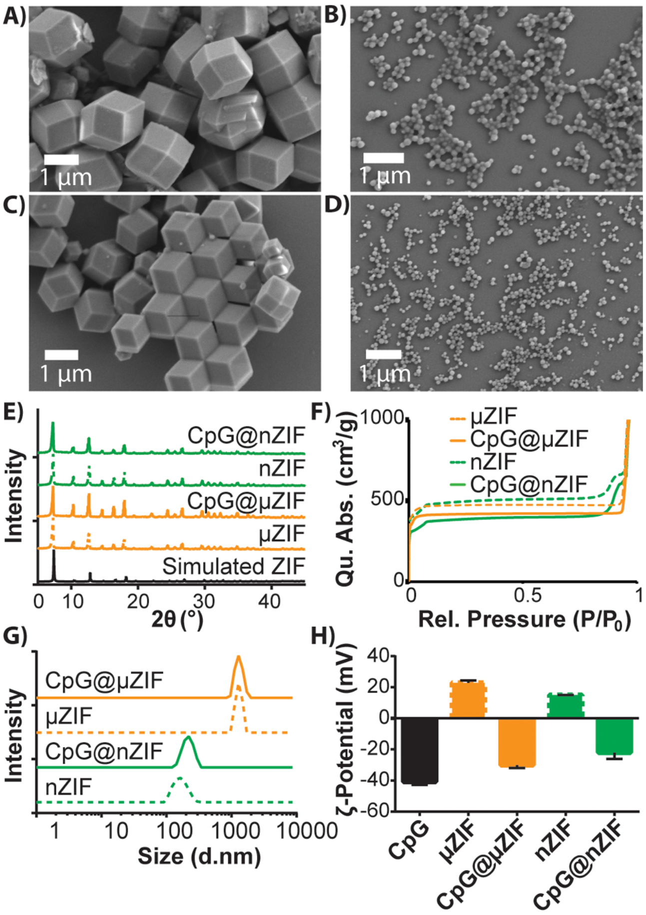


**Figure 1.** Encapsulation of CpG in micro- and nanosized ZIF-8. SEM micrographs of (A) CpG@$\mu$ZIF, (B) CpG@nZIF, (C) pristine $\mu$ZIF, and (D) pristine nZIF. (E) PXRD patterns of CpG@$\mu$ZIF and CpG@nZIF compared to those of pristine and simulated ZIF-8. (F) BET nitrogen isotherms assessing the reduction in the surface area as a result of CpG encapsulation in $\mu$ZIF and nZIF. (G) DLS characterization of the size distribution of CpG@$\mu$ZIF and CpG@nZIF. (H) $\zeta$-potential measurements illustrating the reduction in the negative charge of CpG after encapsulation in the positively charged ZIFs.

which is attributed to the presence of CpG in ZIF-8 (Figure 1F). The hydrodynamic radius of the resulting composites was measured via DLS. From these data, we found CpG@$\mu$ZIF to have a size of around ~1.3 $\mu$m (PDI: 0.374), whereas CpG@nZIF was ~215 nm (PDI: 0.470) (Figure 1G). The ability to control the size of the composites is important in the formulation of vaccines and adjuvants. Polymeric vaccine formulations often advocate for a larger particle size ranging from 500 nm to several microns, with the advantage of providing a sustained release system.[53] With these constructs, we have seen a heightened humoral immune response and prolonged immunity; however, literature reports that particles should be less than 500 nm for optimal uptake by immune cells.[54,55] Having two sizes of CpG@ZIF both above and below this cutoff allows us to make a direct comparison of micro- and nanosized MOFs for optimal delivery of CpG and subsequent activation of B cells. Further characterization of both micro- and nanoformulations found that the encapsulation of CpG in ZIF-8 resulted in a slight shielding of the strong negative charge of the DNA by the positively charged MOF (Figure 1H). It was hypothesized that this factor may also play an important role in mediating cell uptake because mammalian cell membranes are negatively charged owing to the presence of phosphatidyl serine; thus, cargo with strong negative charges are thought to be electrostatically repelled from cell surfaces.[56,57]

To quantitatively and qualitatively confirm DNA encapsulation within ZIF, fluorescently labeled CpG, FITC-CpG, was used. The encapsulation efficiency was first quantified by measuring the amount of unencapsulated material in the supernatant during synthesis. Fluorometric analyses show that CpG was encapsulated quantitatively (~95%; 23−24 $\mu$g of CpG per mL of ZIF) in both sizes of ZIF (Figure 2A,B), an important observation given the high cost of CpG. Qualitatively, confocal images of the micro- and nanoformulations found that the crystals were obviously fluorescent in the FITC channel (Figure 2C). Furthermore, SDS (Figure 2D) and DNase (Figure 2E) washes were employed to remove any surface-bound material. From these experiments, we note that nZIF seems to adsorb CpG onto the surface more than the larger $\mu$ZIF, a phenomenon previously detailed by Li et al.[58] Given the high concentrations of metal and ligand, we were concerned that hydrolysis of the DNA backbone might occur. Curiously, ZIF growth has never been shown to degrade any biomacromolecules, even with such high concentrations of Lewis acids and alkaline ligands. To the contrary, ZIF shells grow and protect even very delicate systems like protein-embedded liposomes,[4] enzymes,[59,60] whole yeast,[61,62] and bacteria.[46,63] To confirm that the CpG was not damaged during the encapsulation, the ZIF shells of CpG@$\mu$ZIF and CpG@nZIF were removed by treatment with 0.5 M EDTA to pull $Zn^{2+}$ from the coating and recover the DNA. Using a 5% agarose gel stained with ethidium bromide, we found that the CpG was unaltered (Figure 2F). After confirming that CpG was properly encapsulated in ZIF-8, we sought to test the ability of ZIF to protect CpG from nuclease degradation. We subjected both CpG@$\mu$ZIF and CpG@nZIF, as well as CpG controls, to DNase I digestion. After incubation with DNase I for 10 min at 37 °C, the CpG@ZIFs samples were exfoliated using 0.5 M EDTA to remove the ZIF shell. The recovered CpG was run on a 5% agarose gel and visualized with ethidium bromide (Figure 2F). It was found that DNase I degraded the unencapsulated CpG, whereas the encapsulated CpG and PS CpG remained intact. This confirms that ZIF successfully protects CpG for nucleases. Furthermore, we tested CpG+ZIF to confirm that the nuclease protection was truly due to the encapsulation of CpG within ZIF (Figure 2F). Mere surface adsorption did not provide the same protection as encapsulation, with complete degradation of CpG observed following the treatment of CpG+ZIF with DNase I. In addition, it was noted that CpG was adsorbed to the surface of nZIF more strongly than $\mu$ZIF, as was made evident by the reduced electrophoretic mobility of CpG, which corroborates our earlier findings.

With our nuclease-resistant formulations of CpG, we then moved *in vitro*. First, we confirmed the biocompatibility of both formulations using an LDH cytotoxicity assay and RAW 264.7 murine macrophages (Figure 3A), where both formulations were found to be nontoxic after a 4 h incubation at the CpG concentrations that we needed to use to induce B cell maturation (3.3 $\mu$g/mL). We then moved forward with cellular assays using splenocytes prepared as a single-cell suspension from spleens of naïve BALB/c mice. Splenocytes are a mixture of T cells, B cells, monocytes, granulocytes,


https://doi.org/10.1021/acsanm.1c03555
ACS Appl. Nano Mater. XXXX, XXX, XXX−XXX

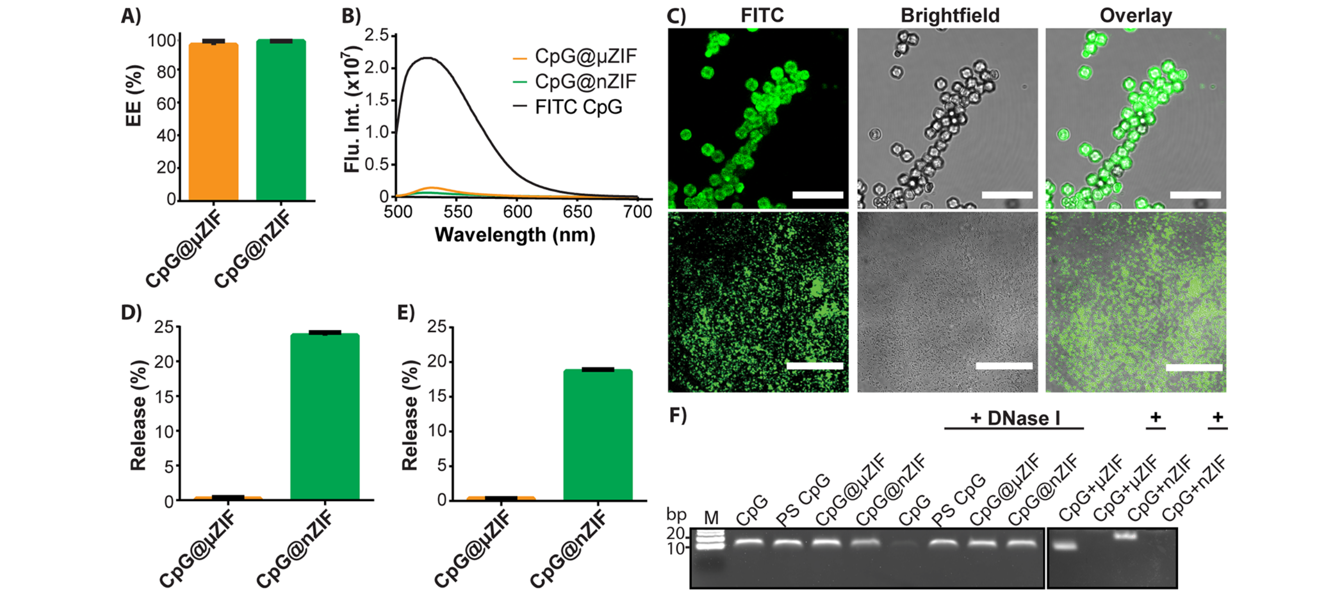


**Figure 2.** Characterization of CpG encapsulated in ZIF-8. (A) Encapsulation efficiency of CpG in ZIF-8 as measured by fluorescence of the supernatant ($n$ = 3; $\lambda_{ex}$ = 495 nm; $\lambda_{em}$ = 520 nm). (B) Representative fluorescence spectra of the supernatant used to measure the encapsulation efficiency ($\lambda_{ex}$ = 495 nm). (C) Confocal images of FITC-labeled CpG@$\mu$ZIF (top, scale bar = 10 $\mu$m) and CpG@nZIF (bottom, scale bar = 20 $\mu$m). (D) Quantification of surface-adsorbed CpG via a SDS wash and fluorescence measurement of the resulting supernatant ($n$ = 3; $\lambda_{ex}$ = 495 nm; $\lambda_{em}$ = 520 nm). (E) Quantification of surface-adsorbed CpG via a DNase wash and fluorescence measurement of the resulting supernatant ($n$ = 3; $\lambda_{ex}$ = 495 nm; $\lambda_{em}$ = 520 nm). (F) 5% agarose gel characterizing the intactness of CpG before and after DNase I digestion to demonstrate the nuclease protection afforded by ZIF encapsulation.

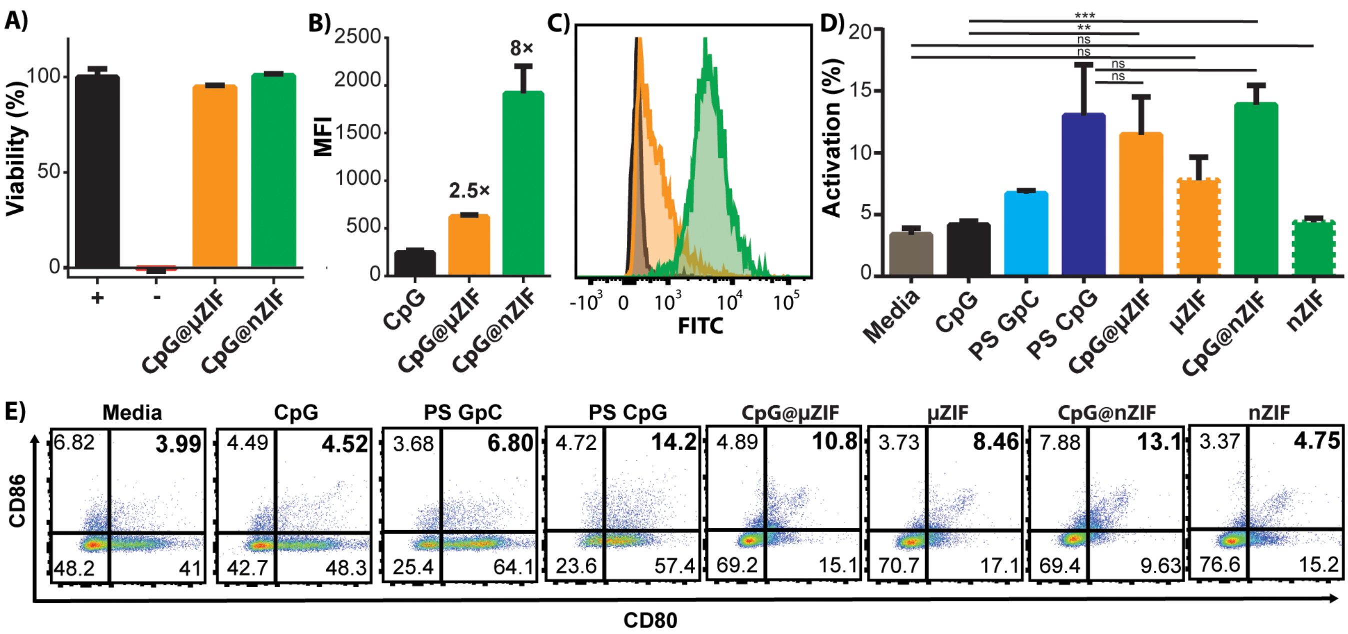


**Figure 3.** Evaluation of micro- and nanosized CpG@ZIF *in vitro*. (A) LDH cytotoxicity assay quantifying the biocompatibility of CpG@$\mu$ZIF and CpG@nZIF with RAW 264.7 murine macrophages after 4 h ($n$ = 3). (B) Uptake of FITC-labeled CpG@$\mu$ZIF and CpG@nZIF by CD19$^+$ B cells after 4 h incubation as measured by flow cytometry ($n$ = 3). (C) Representative histogram of the uptake of FITC-labeled CpG, CpG@$\mu$ZIF, and CpG@nZIF in CD19$^+$ B cells. (D) Percent of activated B cells (CD19$^+$, CD80$^+$, and CD86$^+$) after 48 h of stimulation with CpG@$\mu$ZIF and CpG@nZIF, as measured by flow cytometry ($n$ = 3). (E) Representative flow plots of B cell activation by CpGs and CpG@ZIFs. The statistical significance was calculated by ordinary one-way ANOVA with Tukey's multiple comparison test [*, $p < 0.05$; **, $p < 0.01$; ***, $p < 0.0005$; ****, $p < 0.0001$; ns = not significant ($p > 0.05$)].

dendritic cells, natural killer cells, and macrophages and are commonly used for *in vitro* immune stimulation experiments. Using FITC-labeled CpG, we were able to quantify the uptake of CpG@$\mu$ZIF and CpG@nZIF by B cells using flow cytometry. After incubation of the CpG@ZIFs with splenocytes for 4 h, the cells were washed three times with a low pH buffer to dissolve any surface ZIF.[46,64,65] This ensured that the uptake observed indicated the degree of internalization of the particles. The cells were then stained with Alexa Fluor 700 antimouse CD19 antibody to identify B cells before being


https://doi.org/10.1021/acsanm.1c03555
ACS Appl. Nano Mater. XXXX, XXX, XXX−XXX

analyzed by flow. From these results, we found that both CpG@ZIF formulations were able to improve the uptake of CpG (Figure 3B,C). We attribute this to the improved *in vitro* stability as well as the shielding of the strong negative charge of the DNA by the positively charged carrier. Furthermore, we found that the nanosized formulation, CpG@nZIF, was taken up more efficiently compared with the larger CpG@$\mu$ZIF, following literature examples that nanoparticles are more optimized for cellular uptake. Following uptake by endocytosis, the ZIF is degraded by the acidic pH of the lysosome and releases the CpG cargo to activate B cells.[16,44,45,52,66−68] To test this, we incubated CpG@$\mu$ZIF and CpG@nZIF with splenocytes for 48 h, washed the cells with a low pH buffer, and subsequently stained the cells with three fluorescently labeled antibodies that allow us to differentiate between naïve and activated B cells: Alexa Fluor 700 antimouse CD19 antibody, Alexa Fluor 647 antimouse CD80 antibody, and PE antimouse CD86 antibody. In this study, we employed PS CpG as a positive control and PS GpC, an antisense complement to PS CpG, as a negative control. Using flow cytometry, we were able to quantify B cell activation, where we found that both CpG@$\mu$ZIF and CpG@nZIF were able to improve B cell activation, even matching the performance of the "gold standard" PS CpG (Figure 3D,E). Curiously, despite the significantly enhanced uptake of CpG@nZIF compared to CpG@$\mu$ZIF, there was no significant difference in B cell activation in these two formulations.

## ■ CONCLUSIONS

In this work, we demonstrate how the zinc-based MOF ZIF-8 can be used to encapsulate the ssDNA immunoadjuvant CpG. By tuning the metal-to-ligand ratios, we were able to synthesize both micro- and nanosizes of the encapsulated formulation. Encapsulation of CpG within ZIF-8 was shown to stabilize the PO nucleic acid by protecting it from nuclease degradation. Furthermore, encapsulation of the negatively charged biomacromolecule in the positively charged nanocarrier, ZIF-8, improved the cellular uptake of CpG in B cells, with nanosizes significantly outperforming microsizes. Together, these improvements have demonstrated that ZIF encapsulation has the potential to enhance the function of CpG in adjuvanting an immune response through the activation of B cells to a comparable degree to the state-of-the-art PS CpG. From this work, we hope to shed light on the prospect of using MOFs for the stabilization of PO DNAs.

## ■ AUTHOR INFORMATION

### Corresponding Author

**Jeremiah J. Gassensmith** − *Department of Chemistry and Biochemistry, The University of Texas at Dallas, Richardson, Texas 75080, United States; Department of Biomedical Engineering, The University of Texas at Dallas, Richardson, Texas 75080, United States;* orcid.org/0000-0001-6400-8106; Email: gassensmith@utdallas.edu; www.gassensmithlab.com

### Authors

**Olivia R. Brohlin** − *Department of Chemistry and Biochemistry, The University of Texas at Dallas, Richardson, Texas 75080, United States;* orcid.org/0000-0003-3226-6711

**Ryanne N. Ehrman** − *Department of Chemistry and Biochemistry, The University of Texas at Dallas, Richardson, Texas 75080, United States*

**Fabian C. Herbert** − *Department of Chemistry and Biochemistry, The University of Texas at Dallas, Richardson, Texas 75080, United States*

**Yalini H. Wijesundara** − *Department of Chemistry and Biochemistry, The University of Texas at Dallas, Richardson, Texas 75080, United States*

**Arun Raja** − *Department of Chemistry and Biochemistry, The University of Texas at Dallas, Richardson, Texas 75080, United States*

**Arezoo Shahrivarkevishahi** − *Department of Chemistry and Biochemistry, The University of Texas at Dallas, Richardson, Texas 75080, United States*

**Shashini D. Diwakara** − *Department of Chemistry and Biochemistry, The University of Texas at Dallas, Richardson, Texas 75080, United States*

**Ronald A. Smaldone** − *Department of Chemistry and Biochemistry, The University of Texas at Dallas, Richardson, Texas 75080, United States;* orcid.org/0000-0003-4560-7079

Complete contact information is available at: https://pubs.acs.org/10.1021/acsanm.1c03555

### Author Contributions

O.R.B. optimized the synthesis of CpG@ZIFs and executed SEM, gel electrophoresis, and all *in vitro* studies. F.C.H. performed DLS and $\zeta$ potential characterizations. Y.H.W. performed PXRD characterizations. S.D.D. performed BET nitrogen isotherm experiments under the supervision of R.A.S. R.N.E. performed confocal fluorescence microscopy and fluorimetry experiments and aided in all *in vitro* studies. A.S. also performed fluorimetry experiments. A.R. aided in gel electrophoresis characterizations. O.R.B. and J.J.G. composed the manuscript. J.J.G. conceived the project. All authors have read and given their approval to the final version of the manuscript.

### Funding

J.J.G. acknowledges the National Science Foundation (Grants CAREER DMR-1654405 and DMR-2003534) and Welch Foundation (Grant AT-1989-20190330).

### Notes

The authors declare no competing financial interest.

## ■ REFERENCES

(1) Liang, W.; Xu, H.; Carraro, F.; Maddigan, N. K.; Li, Q.; Bell, S. G.; Huang, D. M.; Tarzia, A.; Solomon, M. B.; Amenitsch, H.; Vaccari, L.; Sumby, C. J.; Falcaro, P.; Doonan, C. J. Enhanced Activity of Enzymes Encapsulated in Hydrophilic Metal-Organic Frameworks. *J. Am. Chem. Soc.* **2019**, *141* (6), 2348−2355.

(2) Wang, C.; Sudlow, G.; Wang, Z.; Cao, S.; Jiang, Q.; Neiner, A.; Morrissey, J. J.; Kharasch, E. D.; Achilefu, S.; Singamaneni, S. Metal-Organic Framework Encapsulation Preserves the Bioactivity of Protein Therapeutics. *Adv. Healthcare Mater.* **2018**, *7* (22), 1800950.

(3) Luzuriaga, M. A.; Welch, R. P.; Dharmarwardana, M.; Benjamin, C. E.; Li, S.; Shahrivarkevishahi, A.; Popal, S.; Tuong, L. H.; Creswell, C. T.; Gassensmith, J. J. Enhanced Stability and Controlled Delivery of MOF-Encapsulated Vaccines and Their Immunogenic Response In Vivo. *ACS Appl. Mater. Interfaces* **2019**, *11* (10), 9740−9746.

(4) Herbert, F. C.; Abeyrathna, S. S.; Abeyrathna, N. S.; Wijesundara, Y. H.; Brohlin, O. R.; Carraro, F.; Amenitsch, H.; Falcaro, P.; Luzuriaga, M. A.; Durand-Silva, A.; Diwakara, S. D.; Smaldone, R. A.; Meloni, G.; Gassensmith, J. J. Stabilization of

supramolecular membrane protein-lipid bilayer assemblies through immobilization in a crystalline exoskeleton. *Nat. Commun.* **2021**, *12*, 2202.
(5) Welch, R. P.; Lee, H.; Luzuriaga, M. A.; Brohlin, O. R.; Gassensmith, J. J. Protein-Polymer Delivery: Chemistry from the Cold Chain to the Clinic. *Bioconjugate Chem.* **2018**, *29* (9), 2867−2883.
(6) Luzuriaga, M. A.; Shahrivarkevishahi, A.; Herbert, F. C.; Wijesundara, Y. H.; Gassensmith, J. J. Biomaterials and nanomaterials for sustained release vaccine delivery. *WIREs Nanomedicine and Nanobiotechnology* **2021**, *13* (6), No. e1735.
(7) Zhou, H.-C.; Long, J. R.; Yaghi, O. M. Introduction to Metal-Organic Frameworks. *Chem. Rev.* **2012**, *112* (2), 673−674.
(8) Zhou, H.-C. J.; Kitagawa, S. Metal-Organic Frameworks (MOFs). *Chem. Soc. Rev.* **2014**, *43* (16), 5415−5418.
(9) Long, J. R.; Yaghi, O. M. The pervasive chemistry of metal-organic frameworks. *Chem. Soc. Rev.* **2009**, *38* (5), 1213−1214.
(10) Ellis, J. E.; Zeng, Z.; Hwang, S. I.; Li, S.; Luo, T.-Y.; Burkert, S. C.; White, D. L.; Rosi, N. L.; Gassensmith, J. J.; Star, A. Growth of ZIF-8 on molecularly ordered 2-methylimidazole/single-walled carbon nanotubes to form highly porous, electrically conductive composites. *Chemical Science* **2019**, *10* (3), 737−742.
(11) Shi, L.; Wu, J.; Qiao, X.; Ha, Y.; Li, Y.; Peng, C.; Wu, R. In Situ Biomimetic Mineralization on ZIF-8 for Smart Drug Delivery. *ACS Biomaterials Science & Engineering* **2020**, *6* (8), 4595−4603.
(12) Lyu, F.; Zhang, Y.; Zare, R. N.; Ge, J.; Liu, Z. One-Pot Synthesis of Protein-Embedded Metal-Organic Frameworks with Enhanced Biological Activities. *Nano Lett.* **2014**, *14* (10), 5761−5765.
(13) Liang, K.; Ricco, R.; Doherty, C. M.; Styles, M. J.; Bell, S.; Kirby, N.; Mudie, S.; Haylock, D.; Hill, A. J.; Doonan, C. J.; Falcaro, P. Biomimetic mineralization of metal-organic frameworks as protective coatings for biomacromolecules. *Nat. Commun.* **2015**, *6*, 7240.
(14) Chen, Y.; Li, P.; Modica, J. A.; Drout, R. J.; Farha, O. K. Acid-Resistant Mesoporous Metal-Organic Framework toward Oral Insulin Delivery: Protein Encapsulation, Protection, and Release. *J. Am. Chem. Soc.* **2018**, *140* (17), 5678−5681.
(15) Zhou, Z.; Gao, Z.; Shen, H.; Li, M.; He, W.; Su, P.; Song, J.; Yang, Y. Metal-Organic Framework in Situ Post-Encapsulating DNA-Enzyme Composites on a Magnetic Carrier with High Stability and Reusability. *ACS Appl. Mater. Interfaces* **2020**, *12* (6), 7510−7517.
(16) Zhang, G.; Fu, X.; Sun, H.; Zhang, P.; Zhai, S.; Hao, J.; Cui, J.; Hu, M. Poly(ethylene glycol)-Mediated Assembly of Vaccine Particles to Improve Stability and Immunogenicity. *ACS Appl. Mater. Interfaces* **2021**, *13* (12), 13978−13989.
(17) Healy, C.; Patil, K. M.; Wilson, B. H.; Hermanspahn, L.; Harvey-Reid, N. C.; Howard, B. I.; Kleinjan, C.; Kolien, J.; Payet, F.; Telfer, S. G.; Kruger, P. E.; Bennett, T. D. The thermal stability of metal-organic frameworks. *Coord. Chem. Rev.* **2020**, *419*, 213388.
(18) Voskanyan, A. A.; Goncharov, V. G.; Novendra, N.; Guo, X.; Navrotsky, A. Thermodynamics Drives the Stability of the MOF-74 Family in Water. *ACS Omega* **2020**, *5* (22), 13158−13163.
(19) Park, K. S.; Ni, Z.; Côté, A. P.; Choi, J. Y.; Huang, R.; Uribe-Romo, F. J.; Chae, H. K.; O'Keeffe, M.; Yaghi, O. M. Exceptional chemical and thermal stability of zeolitic imidazolate frameworks. *Proc. Natl. Acad. Sci. U. S. A.* **2006**, *103* (27), 10186−10191.
(20) Li, S.; Dharmarwardana, M.; Welch, R. P.; Ren, Y.; Thompson, C. M.; Smaldone, R. A.; Gassensmith, J. J. Template-Directed Synthesis of Porous and Protective Core-Shell Bionanoparticles. *Angew. Chem., Int. Ed.* **2016**, *55* (36), 10691−10696.
(21) Li, S.; Gassensmith, J. J. Synthesis of Metal−Organic Frameworks on Tobacco Mosaic Virus Templates. In *Protein Scaffolds: Design, Synthesis, and Applications*; Udit, A. K., Ed.; Springer: New York, 2018; Vol. *1798*, pp 95−108.
(22) Xiong, F.; Qin, Z.; Chen, H.; Lan, Q.; Wang, Z.; Lan, N.; Yang, Y.; Zheng, L.; Zhao, J.; Kai, D. pH-responsive and hyaluronic acid-functionalized metal-organic frameworks for therapy of osteoarthritis. *J. Nanobiotechnol.* **2020**, *18*, 139.
(23) He, L.; Liu, Y.; Lau, J.; Fan, W.; Li, Q.; Zhang, C.; Huang, P.; Chen, X. Recent progress in nanoscale metal-organic frameworks for drug release and cancer therapy. *Nanomedicine* **2019**, *14* (10), 1343−1365.
(24) Luzuriaga, M. A.; Benjamin, C. E.; Gaertner, M. W.; Lee, H.; Herbert, F. C.; Mallick, S.; Gassensmith, J. J. ZIF-8 degrades in cell media, serum, and some—but not all—common laboratory buffers. *Supramol. Chem.* **2019**, *31* (8), 485−490.
(25) Florindo, H. F.; Lopes, J.; Silva, L. C.; Corvo, M. L.; Martins, M. B.; Gaspar, R. Regulatory Development of Nanotechnology-Based Vaccines. In *Micro- and Nanotechnology in Vaccine Development*; Skwarczynski, M., Toth, I., Eds.; William Andrew Publishing, 2017; Chapter 21, pp 393−410.
(26) Wang, Z.-B.; Xu, J. Better Adjuvants for Better Vaccines: Progress in Adjuvant Delivery Systems, Modifications, and Adjuvant-Antigen Codelivery. *Vaccines* **2020**, *8* (1), 128.
(27) Abbasi, S.; Uchida, S. Multifunctional Immunoadjuvants for Use in Minimalist Nucleic Acid Vaccines. *Pharmaceutics* **2021**, *13* (5), 644.
(28) Tizard, I. R. Adjuvants and adjuvanticity. *Vaccines for Veterinarians* **2021**, 75−86.
(29) Pulendran, B.; Arunachalam, P. A.; O'Hagan, D. T. Emerging concepts in the science of vaccine adjuvants. *Nat. Rev. Drug Discovery* **2021**, *20*, 454−475.
(30) Krieg, A. M.; Yi, A. K.; Matson, S.; Waldschmidt, T. J.; Bishop, G. A.; Teasdale, R.; Koretzky, G. A.; Klinman, D. M. CpG motifs in bacterial DNA trigger direct B-cell activation. *Nature* **1995**, *374* (6522), 546−549.
(31) Fehér, K. Single Stranded DNA Immune Modulators with Unmethylated CpG Motifs: Structure and Molecular Recognition by Toll-Like Receptor 9. *Current Protein & Peptide Science* **2019**, *20* (11), 1060−1068.
(32) Ishii, K. J.; Akira, S. Innate immune recognition of nucleic acids: Beyond toll-like receptors. *Int. J. Cancer* **2005**, *117* (4), 517−523.
(33) Jabbari, K.; Bernardi, G. Cytosine methylation and CpG, TpG (CpA) and TpA frequencies. *Gene* **2004**, *333*, 143−149.
(34) Bode, C.; Zhao, G.; Steinhagen, F.; Kinjo, T.; Klinman, D. M. CpG DNA as a vaccine adjuvant. *Expert Review of Vaccines* **2011**, *10* (4), 499−511.
(35) Krug, A.; Rothenfusser, S.; Hornung, V.; Jahrsdörfer, B.; Blackwell, S.; Ballas, Z. K.; Endres, S.; Krieg, A. M.; Hartmann, G. Identification of CpG oligonucleotide sequences with high induction of IFN-alpha/beta in plasmacytoid dendritic cells. *Eur. J. Immunol.* **2001**, *31* (7), 2154−2163.
(36) Hartmann, G.; Weeratna, R. D.; Ballas, Z. K.; Payette, P.; Blackwell, S.; Suparto, I.; Rasmussen, W. L.; Waldschmidt, M.; Sajuthi, D.; Purcell, R. H.; Davis, H. L.; Krieg, A. M. Delineation of a CpG phosphorothioate oligodeoxynucleotide for activating primate immune responses in vitro and in vivo. *J. Immunol.* **2000**, *164* (3), 1617−1624.
(37) Steinhagen, F.; Kinjo, T.; Bode, C.; Klinman, D. M. TLR-based immune adjuvants. *Vaccine* **2011**, *29* (17), 3341−3355.
(38) Shirota, H.; Klinman, D. M. CpG Oligodeoxynucleotides as Adjuvants for Clinical Use. In *Immunopotentiators in Modern Vaccines*, 2nd ed.; Schijns, V. E. J. C., O'Hagan, D. T., Eds.; Academic Press, 2017; Chapter 9, pp 163−198.
(39) van den Boorn, J. G.; Barchet, W.; Hartmann, G. Nucleic Acid Adjuvants: Toward an Educated Vaccine. In *Advances in Immunology*; Melief, C. J. M., Ed.; Academic Press, 2012; Vol. *114*, Chapter 1, pp 1−32.
(40) Senti, G.; Johansen, P.; Haug, S.; Bull, C.; Gottschaller, C.; Müller, P.; Pfister, T.; Maurer, P.; Bachmann, M. F.; Graf, N.; Kündig, T. M. Use of A-type CpG oligodeoxynucleotides as an adjuvant in allergen-specific immunotherapy in humans: a phase I/IIa clinical trial. *Clinical & Experimental Allergy* **2009**, *39* (4), 562−570.
(41) Mutwiri, G. K.; Nichani, A. K.; Babiuk, S.; Babiuk, L. A. Strategies for enhancing the immunostimulatory effects of CpG oligodeoxynucleotides. *J. Controlled Release* **2004**, *97* (1), 1−17.
(42) Hager, S.; Fittler, F. J.; Wagner, E.; Bros, M. Nucleic Acid-Based Approaches for Tumor Therapy. *Cells* **2020**, *9* (9), 2061.

(43) Pohar, J.; Lainšček, D.; Kunšek, A.; Cajnko, M.-M.; Jerala, R.; Benčina, M. Phosphodiester backbone of the CpG motif within immunostimulatory oligodeoxynucleotides augments activation of Toll-like receptor 9. *Sci. Rep.* **2017**, *7*, 14598.
(44) Zhang, Y.; Wang, F.; Ju, E.; Liu, Z.; Chen, Z.; Ren, J.; Qu, X. Metal-Organic-Framework-Based Vaccine Platforms for Enhanced Systemic Immune and Memory Response. *Adv. Funct. Mater.* **2016**, *26* (35), 6454−6461.
(45) Poddar, A.; Conesa, J. J.; Liang, K.; Dhakal, S.; Reineck, P.; Bryant, G.; Pereiro, E.; Ricco, R.; Amenitsch, H.; Doonan, C.; Mulet, X.; Doherty, C. M.; Falcaro, P.; Shukla, R. Encapsulation, Visualization and Expression of Genes with Biomimetically Mineralized Zeolitic Imidazolate Framework-8 (ZIF-8). *Small* **2019**, *15* (36), 1902268.
(46) Luzuriaga, M. A.; Herbert, F. C.; Brohlin, O. R.; Gadhvi, J.; Howlett, T.; Shahrivarkevishahi, A.; Wijesundara, Y. H.; Venkitapathi, S.; Veera, K.; Ehrman, R.; Benjamin, C. E.; Popal, S.; Burton, M. D.; Ingersoll, M. A.; De Nisco, N. J.; Gassensmith, J. J. Metal-Organic Framework Encapsulated Whole-Cell Vaccines Enhance Humoral Immunity against Bacterial Infection. *ACS Nano* **2021**, *15* (11), 17426−17438.
(47) Li, S.; Zhou, X.; Chen, Z.; Herbert, F. C.; Jayawickramage, R.; Panangala, S. D.; Luzuriaga, M. A.; Alahakoon, S. B.; Diwakara, S. D.; Meng, X.; Fei, L.; Ferraris, J.; Smaldone, R. A.; Gassensmith, J. J. Hierarchical Porous Carbon Arising from Metal-Organic Framework-Encapsulated Bacteria and Its Energy Storage Potential. *ACS Appl. Mater. Interfaces* **2020**, *12* (10), 11884−11889.
(48) Hou, X.; Zaks, T.; Langer, R.; Dong, Y. Lipid nanoparticles for mRNA delivery. *Nature Reviews Materials* **2021**, *6*, 1078−1094.
(49) Donaldson, B.; Lateef, Z.; Walker, G. F.; Young, S. L.; Ward, V. K. Virus-like particle vaccines: immunology and formulation for clinical translation. *Expert Review of Vaccines* **2018**, *17* (9), 833−849.
(50) Yeh, M.-K.; Chang, H.-I.; Cheng, M.-Y. Clinical development of liposome-based drugs: formulation, characterization, and therapeutic efficacy. *Int. J. Nanomed.* **2011**, *7*, 49−60.
(51) Chen, T.-T.; Yi, J.-T.; Zhao, Y.-Y.; Chu, X. Biomineralized Metal-Organic Framework Nanoparticles Enable Intracellular Delivery and Endo-Lysosomal Release of Native Active Proteins. *J. Am. Chem. Soc.* **2018**, *140* (31), 9912−9920.
(52) Zhang, H.; Chen, W.; Gong, K.; Chen, J. Nanoscale Zeolitic Imidazolate Framework-8 as Efficient Vehicles for Enhanced Delivery of CpG Oligodeoxynucleotides. *ACS Appl. Mater. Interfaces* **2017**, *9* (37), 31519−31525.
(53) Lee, B. K.; Yun, Y.; Park, K. PLA micro- and nano-particles. *Adv. Drug Delivery Rev.* **2016**, *107*, 176−191.
(54) Silva, A. L.; Soema, P. C.; Slütter, B.; Ossendorp, F.; Jiskoot, W. PLGA particulate delivery systems for subunit vaccines: Linking particle properties to immunogenicity. *Human Vaccines & Immunotherapeutics* **2016**, *12* (4), 1056−1069.
(55) Sousa de Almeida, M.; Susnik, E.; Drasler, B.; Taladriz-Blanco, P.; Petri-Fink, A.; Rothen-Rutishauser, B. Understanding nanoparticle endocytosis to improve targeting strategies in nanomedicine. *Chem. Soc. Rev.* **2021**, *50* (9), 5397−5434.
(56) Yeung, T.; Gilbert, G. E.; Shi, J.; Silvius, J.; Kapus, A.; Grinstein, S. Membrane Phosphatidylserine Regulates Surface Charge and Protein Localization. *Science* **2008**, *319* (5860), 210−213.
(57) Ma, Y.; Poole, K.; Goyette, J.; Gaus, K. Introducing Membrane Charge and Membrane Potential to T Cell Signaling. *Frontiers in Immunology* **2017**, *8*, 1513.
(58) Li, S.; Dharmarwardana, M.; Welch, R. P.; Benjamin, C. E.; Shamir, A. M.; Nielsen, S. O.; Gassensmith, J. J. *ACS Appl. Mater. Interfaces* **2018**, *10* (21), 18161−18169.
(59) Wang, Y.; Zhang, N.; Tan, D.; Qi, Z.; Wu, C. Facile Synthesis of Enzyme-Embedded Metal-Organic Frameworks for Size-Selective Biocatalysis in Organic Solvent. *Frontiers in Bioengineering and Biotechnology* **2020**, *8*, 714.
(60) Ricco, R.; Wied, P.; Nidetzky, B.; Amenitsch, H.; Falcaro, P. Magnetically responsive horseradish peroxidase@ZIF-8 for biocatalysis. *Chem. Commun.* **2020**, *56* (43), 5775−5778.
(61) Liang, K.; Richardson, J. J.; Cui, J.; Caruso, F.; Doonan, C. J.; Falcaro, P. Metal-Organic Framework Coatings as Cytoprotective Exoskeletons for Living Cells. *Adv. Mater.* **2016**, *28* (36), 7910−7914.
(62) Sun, C.; Chang, L.; Hou, K.; Liu, S.; Tang, Z. Encapsulation of live cells by metal-organic frameworks for viability protection. *Science China Materials* **2019**, *62* (6), 885−891.
(63) Yan, S.; Zeng, X.; Wang, Y.; Liu, B.-F. Biomineralization of Bacteria by a Metal-Organic Framework for Therapeutic Delivery. *Adv. Healthcare Mater.* **2020**, *9* (12), 2000046.
(64) Galeotti, C.; Karnam, A.; Das, M.; Kaveri, S. V.; Bayry, J. Acid Stripping of Surface IgE Antibodies Bound to FcεRI Is Unsuitable for the Functional Assays That Require Long-Term Culture of Basophils and Entire Removal of Surface IgE. *International Journal of Molecular Sciences* **2020**, *21* (2), 510.
(65) Kameyama, S.; Horie, M.; Kikuchi, T.; Omura, T.; Tadokoro, A.; Takeuchi, T.; Nakase, I.; Sugiura, Y.; Futaki, S. Acid wash in determining cellular uptake of Fab/cell-permeating peptide conjugates. *Peptide Science* **2007**, *88* (2), 98−107.
(66) Sun, C.-Y.; Qin, C.; Wang, X.-L.; Yang, G.-S; Shao, K.-Z.; Lan, Y.-Q.; Su, Z.-M.; Huang, P.; Wang, C.-G.; Wang, E.-B. Zeolitic imidazolate framework-8 as efficient pH-sensitive drug delivery vehicle. *Dalton Transactions* **2012**, *41* (23), 6906−6909.
(67) Zhong, X.; Sun, X. Nanomedicines based on nanoscale metal-organic frameworks for cancer immunotherapy. *Acta Pharmacol Sin* **2020**, *41*, 928−935.
(68) Abdelhamid, H. N.; Dowaidar, M.; Hällbrink, M.; Langel, Ü. Gene delivery using cell penetrating peptides-zeolitic imidazolate frameworks. *Microporous Mesoporous Mater.* **2020**, *300*, 110173.